AGU PUBLICATIONS

JGR

Journal of Geophysical Research: Space Physics

RESEARCH ARTICLE
10.1002/2016JA023521

Special Section:
Major Results From the MAVEN Mission to Mars

This article is a companion to *Brecht et al.* [2017] doi:10.1002/2016JA023510.

Key Points:
- Ion escape rates from the simulations are in agreement with MAVEN
- The assumptions used to scale the MAVEN ion fluxes to account for unsampled regions are valid
- Scaling the MAVEN ion escape rates to account for ions of all kinetic energies gives a total heavy ion escape rate of 1.2×10^{24} ions/s

Correspondence to:
S. A. Ledvina,
ledvina@ssl.berkeley.edu

Citation:
Ledvina, S. A., S. H. Brecht, D. A. Brain, and B. M. Jakosky (2017), Ion escape rates from Mars: Results from hybrid simulations compared to MAVEN observations, *J. Geophys. Res. Space Physics*, *122*, doi:10.1002/2016JA023521.

Received 26 SEP 2016
Accepted 28 JUN 2017
Accepted article online 7 JUL 2017

Ion escape rates from Mars: Results from hybrid simulations compared to MAVEN observations

Stephen A. Ledvina[1], Stephen H. Brecht[2], David A. Brain[3], and Bruce M. Jakosky[3]

[1]Space Sciences Laboratory, UC, Berkeley, California, USA, [2]Bay Area Research Corp, Orinda, California, USA, [3]Laboratory for Atmospheric and Space Physics, University of Colorado Boulder, Boulder, Colorado, USA

Abstract Daily averaged heavy ion escape rates from HALFSHEL hybrid simulations of the solar wind interaction with the Martian ionosphere are compared to the ion escape rates reported by Brain et al. (2015). The simulation rates are found to be in agreement with the rates measured by Mars Atmosphere and Volatile EvolutioN (MAVEN). When the simulation rates are adjusted for known variability in the Martian system, the ion escape rates are within 40% of the MAVEN results. The ion escape rate is found to vary linearly with the solar wind speed. Using the simulation results to scale the MAVEN ion escape rate to include ions of all kinetic energies, we predict a total heavy ion escape rate of 1.2×10^{25} ions/s. The assumptions used to derive the total ion escape by Brain et al. (2015) are tested against the simulation results and are found to be excellent.

1. Introduction

It is thought that Mars was once a wet world with large bodies of liquid water on its surface [cf. *Lasue et al.*, 2013]. Today, that is not the case leading to the question, "Where did the water go?" There are two obvious answers: into the surface of the planet or lost to space [cf. *Lammer et al.*, 2013]. The objective of the Mars Atmosphere and Volatile EvolutioN (MAVEN) mission is to address the loss of the Martian atmosphere and hence, the loss of water to space [*Jakosky et al.*, 2015]. Atmospheric escape can be broken down into two classifications: neutral escape and ion escape. This paper focuses on the latter.

Ion escape from Mars has been a topic of interest for many years. The first estimates for the ion escape came from Phobos-2. More recently, the Mars Express (MEX) mission has spent over a decade (since 2004) measuring ion fluxes around Mars and providing estimates for the ion escape rates [cf. *Ramstad et al.*, 2015; *Nilsson et al.*, 2010; *Barabash et al.*, 2007, and references therein]. Measured estimates of the ion escape rates vary from a 2×10^{23}–3×10^{25} ions/s. A compilation of pre-MAVEN ion escape rates versus the EUV flux ($F_{10.7}$) was published by *Lundin et al.* [2013].

Two distinct numerical approaches have been employed to estimate the ion escape rate from Mars. The first is the MHD formalism [cf. *Liu et al.*, 2001; *Ma et al.*, 2002, 2004, 2015; *Ma and Nagy*, 2007; *Harnett and Winglee*, 2006; *Dong et al.*, 2014, 2015]. The second is the kinetic formalism, specifically the hybrid particle code [cf. *Brecht*, 1990; *Brecht and Ferrante*, 1991; *Kallio and Janhunen*, 2002; *Bößwetter et al.*, 2004; *Modolo et al.*, 2005, 2016; *Holmstrom and Wang*, 2015; *Brecht et al.*, 2016, 2017]. In addition to these two fundamental approaches an ion tracking approach using the electric and magnetic fields from a MHD simulation has also been used [cf. *Cravens et al.*, 2002; *Fang et al.*, 2010a, 2010b; *Curry et al.*, 2014]. The ion tracking approach attempts to capture some of the ion kinetic behavior not present in MHD simulations. The disadvantage of this method is that the ion motion and the fields are not self-consistent. A detailed discussion of the implicit assumptions, limitations, and application of each approach can be found in *Ledvina et al.* [2008].

The MAVEN mission carries the most complete and sophisticated suite of plasma and fields instruments ever flown to Mars. Utilizing several of these instruments, *Brain et al.* [2015] determined the spatial distribution of the ion fluxes around Mars and placed a lower limit of 2.8×10^{24} ions/s on the heavy ion (greater than 9 amu) escape rate (the MAVEN escape rate). This rate is a lower limit because the contribution ions with a kinetic energy (KE) < 25 eV were neglected. It took several months worth of data to arrive at that rate. During that time the effects of several parameters on the ion escape rate had to be averaged over.

The magnetic and electric fields carried by the solar wind drive ion loss from Mars. The solar wind consists of protons streaming past Mars with a nominal speed of $|\boldsymbol{v}_{sw}| = 300$–$500$ km/s. Moving along with the solar wind is the interplanetary magnetic field (IMF), $|\boldsymbol{B}| \sim 3$ nT and the convection electric field, $\boldsymbol{E}_{conv} = -\boldsymbol{v}_{sw} \times \boldsymbol{B}$ (see Figure 1a). The convection electric field acting on the ionosphere accelerates ions away from Mars and has

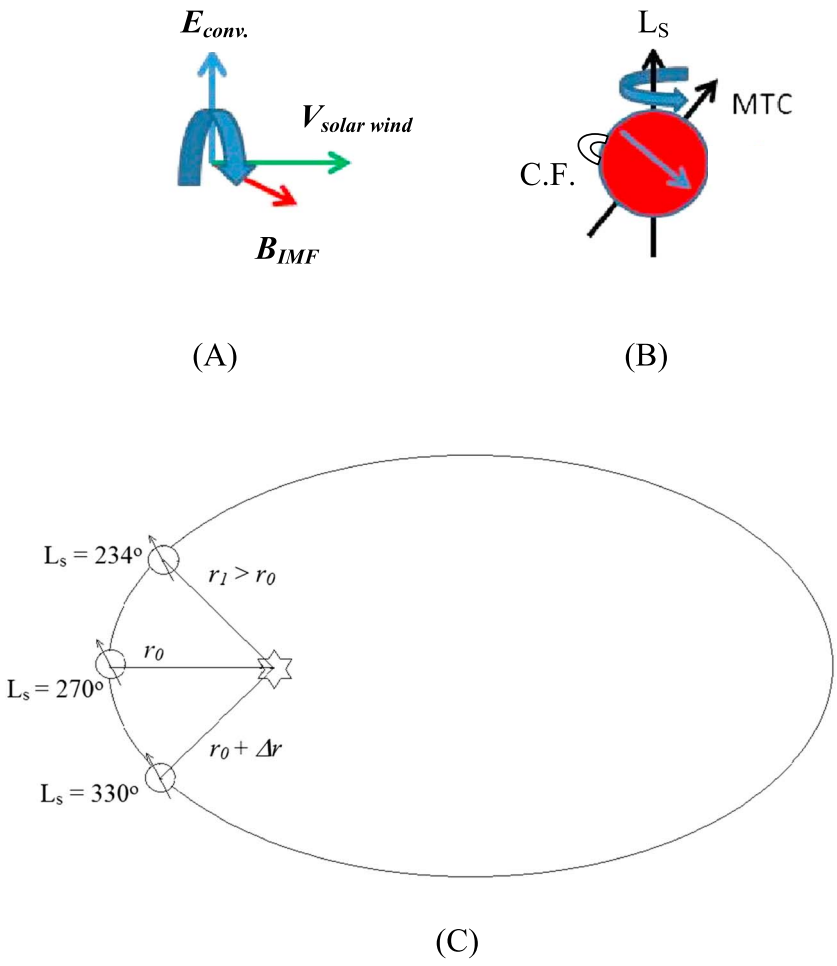

Figure 1. Variables in the Martian solar wind interaction. (a) The direction and magnitude of the interplanetary magnetic field ($\boldsymbol{B}_{\mathbf{IMF}}$) and the convection electric field ($\boldsymbol{E}_{\mathbf{conv}}$) can change over time. (b) The orientation of the crustal magnetic fields (C.F.) with respect to the solar wind changes with planet rotation. (c) Illustration of the position of Mars during the MAVEN data collection period. Mars was at a distance r_1 when MAVEN began collecting data. During the data collection time Mars moved through perihelion (r_0) and out to a distance of $r_0 + \Delta r$ at the end of the data collection time.

been shown to organize the ion data [*Dubinin et al.*, 2008]. To study ion loss from Mars, it is natural to use a coordinate system that is aligned with the convection electric field. The Mars Solar Electric (MSE) coordinate system is centered on Mars and defined to have the *x* axis pointing into the incident solar wind direction (generally toward the Sun), the *y* axis points along the direction of the component of the IMF perpendicular to the solar wind velocity, and the *z* axis is aligned with the convection electric field. The MSE coordinate system is tied to the solar wind's electric and magnetic fields. As the directions of the fields change so to does the orientation of the MSE coordinate system. The simulations have the solar wind coming straight from the Sun, so X_{MSE} is along the Mars-Sun line.

Unlike other nonmagnetized bodies with atmospheres such as Venus and Titan, Mars has localized crustal magnetic fields. The presence of the crustal fields complicates the solar wind interaction and has a significant impact on ion escape from Mars [cf. *Ramstad et al.*, 2016; *Brecht et al.*, 2016; *Dong et al.*, 2015; *Ma et al.*, 2015; *Brecht and Ledvina*, 2012, 2014]. As the planet rotates during the Martian day different crustal fields are exposed or sheltered from the solar wind. The rotation angle of Mars is defined by Coordinated Mars Time (MTC), which is the longitude of Mars that goes through the subsolar point (see Figure 1b). A MTC = 0° has the Martian prime meridian pointed at the Sun. Like Earth, the Martian rotation axis is tilted by ~25° from perpendicular to the ecliptic. The tilted axis is responsible for the Martian seasons and also changes the orientation of the crustal magnetic fields relative to the MSE coordinate system. The orientation of the Martian rotation axis is defined by the parameter L_S, where L_S = 0°, 90°,

180°, and 270° corresponds to spring equinox, summer solstice, fall equinox, and winter solstice in the northern hemisphere (Figure 1c).

Several aspects of the Martian plasma environment make understanding ion loss at Mars challenging. The solar activity (EUV flux) is not constant and varies considerably over time; as it varies so does the photoionization rates in the Martian atmosphere. Further complexities arise because of the eccentricity of the Martian orbit. Even if the solar activity (EUV flux) was constant, the photoionization rates at Mars will vary because the orbit of Mars is not circular. As Mars moves along its orbit it also moves radially toward and away from the Sun; the EUV intensity at Mars varies as $1/r^2$, where r is the distance from Mars to the Sun. The EUV flux at Mars drops ~30% when the planet moves between perihelion and aphelion.

The Sun emits a varying solar wind, with changing density and speed, and an ever changing IMF vector. The changing IMF vector and solar wind velocity result in an ever changing $\boldsymbol{E}_{\mathbf{conv}}$. Thus, the MSE coordinate system is constantly changing orientation. In short several aspects of the Martian environment make understanding the ion loss rates from Mars challenging because the loss rates are dependent on each of these parameters. Comparing a few simulations to the loss rates derived from months worth of measurements is not straightforward.

The next section of this paper will review the process *Brain et al.* [2015] used to derive the heavy ion escape rates from the MAVEN data. This will be followed by a discussion of the simulations that were performed. The simulation results will be compared to the *Brain et al.* [2015] results and reported in section 4. Section 5 will discuss the results, their implications for future MAVEN observations of ion escape, and their implications of our understanding of ion loss from Mars.

2. The MAVEN Determination of Ion Escape

MAVEN carries the most complete and sophisticated set of plasma and field instruments ever flown to Mars, yet each of MAVEN's instruments has their own limitations. The instrumental field of view does not cover a full 4π sr. Detecting particles at low kinetic energies can be hampered by surface charges carried by the instruments or the spacecraft. It can take several seconds for an instrument to collect data and arrive at a meaningful measurement. In that time the spacecraft can move several kilometers, effectively smoothing out features over that distance. It will take MAVEN a long time to sample the entire Martian atmosphere/ionosphere. It is not possible for MAVEN to know the unperturbed upstream conditions; at the same time, observations are being made within the planet's atmosphere or downstream of the interaction. One must make the assumption that the incident solar wind conditions have not changed much since they were last sampled. This single observation point limitation can be relaxed to some extent if the MAVEN observations are used in conjunction with the plasma observations made by MEX. Though this has yet to be done, it could be a very enlightening exercise.

All these issues combined make it difficult to collect a global set of observations under the same incident conditions and to separate the effects of various drivers on the Martian ion escape rate. In spite of all these difficulties, *Brain et al.* [2015] succeeded in placing a lower limit on the heavy ion (greater than 9 amu) escape rate. To overcome these uncertainties, several steps and assumptions were made.

Data were collected from 16 November 2014 through 1 April 2015 (4.5 months), when MAVEN was located between 1.25 and 1.45 R_M from Mars. The data spanned a limited range of coverage relative to the Martian geography. On an orbit by orbit bases each measurement was transformed into the MSE coordinate system using the best estimate of the upstream IMF and solar wind directions from the magnetometer [*Connerney et al.*, 2014, 2015] and the solar wind ion analyzer [*Halekas et al.*, 2013]. The measurements were then mapped to a spherical shell around Mars in the MSE frame increasing the data coverage to approximately 68% of the surface area of the sampling shell. A total of 20,836 observations of ion fluxes from the suprathermal and thermal ion composition instrument [*McFadden et al.*, 2015] were used. Ions with a kinetic energy (KE) of less than 25 eV were removed from the data to account for the difficulties associated with measuring low-energy ions. *Brain et al.* [2015] quote an overall uncertainty in the determination of the ion flux to be 50% or less (the energy limit not withstanding).

The ion flux through the sampling shell was further subdivided into four regions: dayside, nightside $+\boldsymbol{E}$ and $-\boldsymbol{E}$, and each region subdivided into 5° × 5° bins. A schematic of the regions is shown in Figure 2. The $+\boldsymbol{E}$ region extends from 45 to 90° latitude, the unperturbed convection electric field points away from the planet in this region. The unperturbed convection electric field points toward the planet in the $-\boldsymbol{E}$ region extending

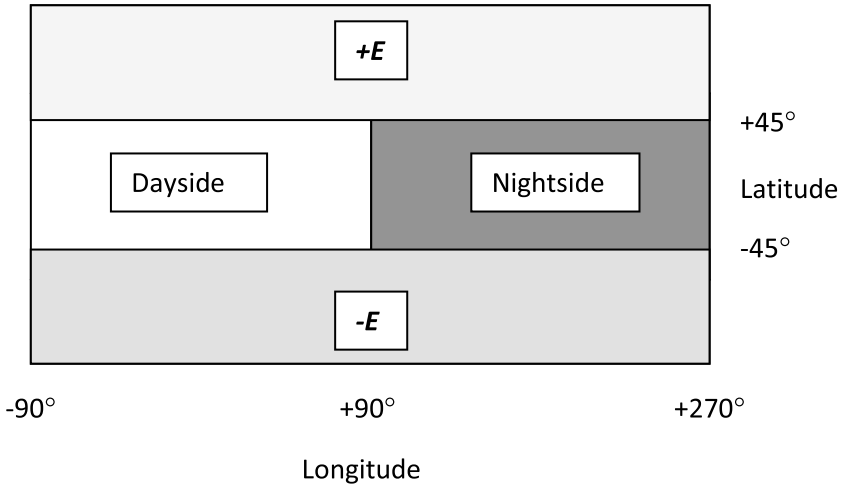

(A)

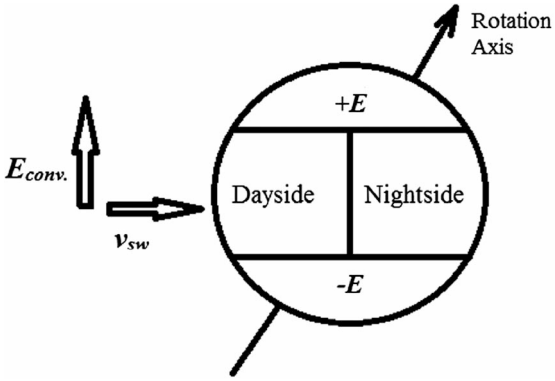

(B)

Figure 2. A schematic showing the ion loss regions defined by *Brain et al.* [2015], a (a) two-dimensional projection and (b) wrapped around Mars. The unperturbed convection electric field points away from Mars in the ***+E*** region and points toward Mars in the ***−E*** region.

from latitudes −45° to −90°, the remaining region between latitudes of ±45° was split into dayside and nightside regions. The dayside covers between ±90° longitudes. This was done to evaluate the heavy ion flux both leaving and approaching the planet and to distinguish a potential ion plume of escaping ions.

Approximately 68% of the surface area of the sampling shell around Mars in the MSE frame was sampled by MAVEN. To account for the ion escape from the unsampled regions, it was assumed that the sampled radially outward moving heavy ion flux on average was representative of the flux from the unsampled regions. The outward heavy ion escape rates were then scaled up by 32% to account for ion escape from regions not sampled by MAVEN. Based on test-particle calculations, it was assumed that the inward ion flux on the nightside of the planet originated below the sampling shell on the dayside. Radially inward fluxes in the remaining regions were assumed to have originated above the sampling shell in the hot O corona and were not counted as ionospheric loss. Therefore, only the nightside inward moving flux was scaled for the nightside coverage and subtracted from the scaled outward heavy ion flux. The resulting heavy ion escape rate from Mars was found to be 2.8×10^{24} ions/s. This is a lower limit for the heavy ion escape rate since ions with KE $<$ 25 eV were ignored.

The ion fluxes measured by MAVEN in the MSE frame are shown in Figure 3. Regions where MAVEN collected no data are shown in grey. The median ion flux collected in each 5° × 5° sampling bin is shown. The median radially moving inward flux is shown in Figure 3 (top). The radially outward moving ion flux is shown in

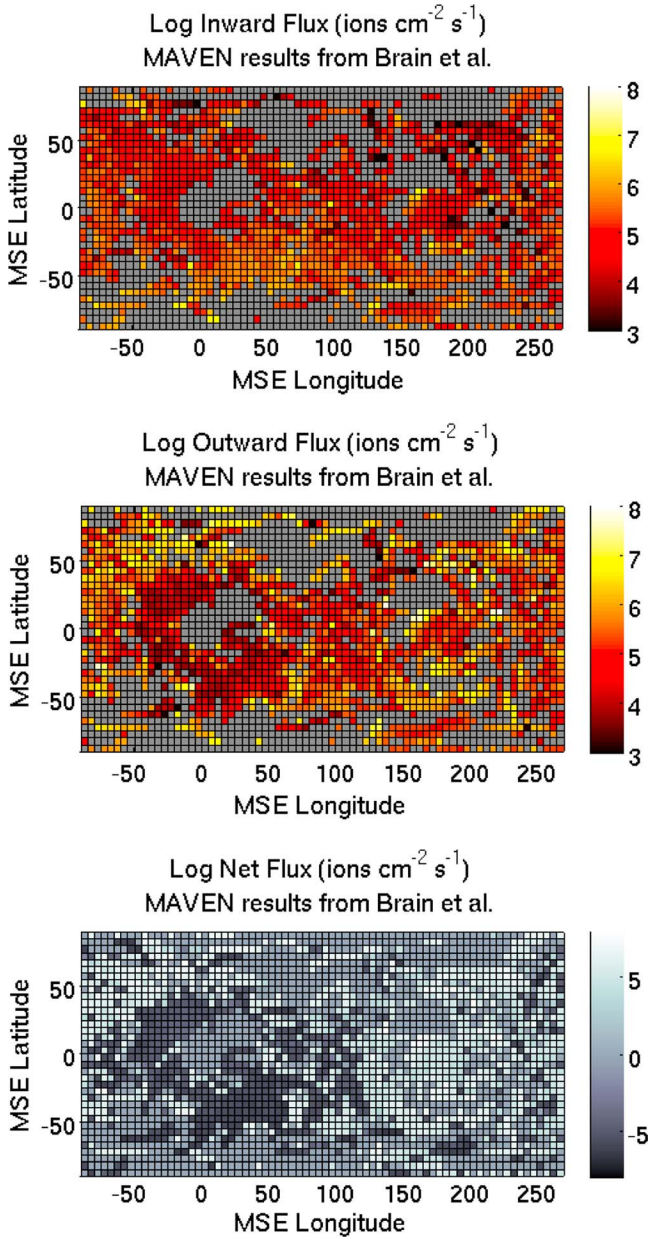

Figure 3. Shown are the ion fluxes measured by MAVEN from *Brain et al.* [2015], for ions with KE > 25 eV: (top) radially inward moving flux, (middle) radially outward moving flux, and (bottom) net flux, outward-inward. Bins where MAVEN collected no data are in gray in the top two plots and set to 0 in the bottom plot.

Figure 3 (middle). The outward moving flux is lowest in the dayside region. Figure 3 (bottom) shows the net flux in each bin found by differencing the outward flux and the inward flux. The net flux is outward on the nightside of the planet and at high latitudes, while the net flux is toward the planet on the dayside.

During the 4.5 months that MAVEN collected data the solar activity was not constant. MAVEN is able to measure the EUV flux at Mars but that data are not currently available. However, monthly averages of the EUV flux measured at the Earth during that time show a downward trend in the EUV flux. The monthly averaged $F_{10.7}$ index is ~160 at the start of the data collection. By the end the $F_{10.7}$ index is down near 120. Daily averages of the EUV flux show an even greater variation with several days in a row where the $F_{10.7}$ index is at 200 and a few below 110. The effects of the changing EUV flux during the MAVEN observation time on the Martian ionosphere are discussed by *Benna et al.* [2015].

Over the 4.5 months of data collection the distance between the Sun and Mars increased by 1.1×10^{11} km; this further reduces the effective EUV flux at Mars. During this time the L_S went from 234° to 334°, thus changing the orientation of the poles (rotation axis of the planet) with respect to the subsolar point. The solar wind parameters were not constant during this time. The solar wind speed measured by MAVEN varied from ~300 km/s to over 600 km/s [*Halekas et al.*, 2015]. The MAVEN coverage in the MSE coordinate system shows that the convection electric field underwent at least one full rotation during the data collection period [*Brain et al.*, 2015]. It is not practical to run a simulation of the Martian solar wind interaction that spans 4.5 months of time and to realistically vary each of the above conditions. However, to make a reasonable comparison to the MAVEN observations, these variations were addressed.

3. Simulation Details

The research reported here uses the HALFSHEL hybrid particle code to simulate the Martian solar wind interaction (see *Brecht et al.* [2016] for a detailed description and history of HALFSHEL). HALFSHEL simulations of

the Martian solar wind interaction have been increasing in complexity over the last several years. Its latest incarnation is the only simulation set that has been shown to agree with the Martian ion loss data versus solar EUV flux as reported by *Lundin et al.* [2013] [see *Brecht et al.*, 2016; *Brecht and Ledvina*, 2014].

Like observations, simulations make many assumptions such as choosing what models to include, design decisions made in selecting a scheme to solve them, and approximations made implementing the selected scheme into code. The implicit assumptions made in the HALFSHEL simulations of Martian solar wind interaction can be found in *Brecht et al.* [2016] and *Brecht and Ledvina* [2012, 2014, references therein]. A review of the hybrid formalism and its implicit assumptions can be found in *Ledvina et al.* [2008]. The HALFSHEL code has been used and tested on a wide variety of problems. The interested reader is referred to *Brecht et al.* [2016 and references therein].

Several models have been added to HALFSHEL in order to simulate the Martian solar wind interaction. They will be briefly mentioned here. Further details about the models and their testing can be found in *Brecht et al.* [2016]. The following models are included within HALFSHEL.

1. Multiple ion species. Each ion species is self-consistently transported with the self-consistent electric and magnetic fields. In this simulation H^+ represents the solar wind, and O^+ and $O_2{}^+$ represent the ionosphere. Additionally, a fourth ionospheric species, $CO_2{}^+$, is evolved chemically but is treated as a stationary species.
2. A neutral atmosphere model. The densities of neutral CO_2 and O as well as their motion (winds) were provided by the Mars Thermospheric General Circulation Model (MTGCM) [e.g., *Bougher et al.*, 1988, 1999a, 1999b, 2000, 2002, 2004, 2006, 2008].
3. A ion-neutral photo-driven non-local thermodynamic equilibrium (LTE) chemistry package. The upper ionosphere is not in local thermodynamic equilibrium (non-LTE) due to plasma transport. The ion-neutral chemistry package evolves a set of ion-neutral chemical reactions in a time accurate fashion. The chemical reactions and their rates are the same as used by other authors [cf. *Brecht and Ledvina*, 2012; *Ma et al.*, 2002, 2004]. The ion-neutral reactions are solved on a spherical grid with a radial spacing of 10 km and an angular spacing of 1.4°. The spherical grid extends from 150 to 1000 km altitude (or 1.04 to 1.29 R_M). Another spherical grid is used to represent ionization of the hot O corona. This grid extends to 2 R_M in altitude with a radial spacing of 100 km.
4. A ion-neutral collisional drag model. This model addresses species by species collisions using the spherical grid. The HALFSHEL code treats the ion drag by individually colliding the H^+, O^+, and $O_2{}^+$ particles with atmospheric CO_2 and O using their respective collision cross sections, densities, and velocity dependence. Currently, heating of the particles, thermalization (randomization) of their trajectories is not included. The interaction is simply an energy loss (drag) from the particles being tracked. The neutral densities are untouched as mentioned earlier; thus, the energy transfer to the neutrals is not included in the simulations.
5. A conductivity model. Hall and Pedersen conductivities are included in the electric field solutions. The generalized electric field including the Hall and Pedersen terms comes from a text by *Mitchner and Kruger* [1973]. In the limit that the collision frequencies go to zero, this equation returns to the normal electric field equation found in a hybrid particle code [*Brecht and Thomas*, 1988].
6. A crustal magnetic field model. The model used is from *Purucker et al.* [2000].
7. Planetary geometry package. The inclusion of the crustal fields and the neutral winds into the simulations made it necessary to include planetary rotation during the simulations along with the L_S orientation. This is consistent with the orientation of the MTGCM that includes the orientation and tilt of the Martian rotation axis.

Ion escape rates from HALFSHEL hybrid simulations of the Martian solar wind interaction are not a constant value. Indeed, hybrid simulations never truly come into steady state like MHD or MHD+ test-particle simulations. The plasma wave families present in the code (kinetic Alfvén waves, electromagnetic ion cyclotron waves, whistlers etc…) together with the planet's rotation and the responding ionospheric chemistry lead to an unsteady outflow of ions from the Martian ionosphere. Examples of the effects these variations have on ion loss will be discussed later in the paper.

The research reported in this paper made use of five simulations. Four of the simulations represented the orientations of the MTC (0°, 90°, 180°, and 270°). Each used the following solar wind conditions: H^+ density

of 2.7 cm^{-3}, with a speed of 485 km/s, and an electron temperature of 9 eV. The interplanetary magnetic field (IMF) had a magnitude of 3 nT and a Parker spiral angle of 56°. These conditions chosen are typical solar wind conditions based several years of MEX and MGS observations [*Brain et al.*, 2012]. Photoionization rates consistent with a $F_{10.7}$ flux of 130 extrapolated to the Martian location were used. The planet's rotation axis was tilted at an angle of 25.19°, orientated at L_S = 270° (summer in the southern hemisphere). These conditions were consistent with those present during December of 2014 shortly after MAVEN began taking data. The simulations were run for 2000 s real time during which the planet rotated through 8.3°. Each simulation was run until the average loss rates reached a steady state. The simulations were performed using the best inputs and models available prior to the start of the MAVEN mission. The simulations were completed before the published MAVEN results. No attempt has been made to tune the input parameters of the simulations to better match the MAVEN results. However, scaling of the results of the simulations to represent parameters encountered by MAVEN is undertaken in the following portions of the paper.

A fifth simulation is used to check the scaling of ion loss rates with the solar wind speed. The parameters for that run are identical to the MTC = 270° mentioned above except that a solar wind speed of 400 km/s was used. The solar wind data observed by MAVEN at Mars and reported by *Halekas et al.* [2015] suggest a lower average speed than the 485 km/s used in the four simulations would be a better choice.

All of the simulations used the same MSE coordinate system defined by the solar wind speed and IMF mentioned above. A spherical shell was set up around the planet at 1.35 R_M in the MSE coordinate system. Note that the planetary rotation axis is not aligned with the MSE coordinate system used in the simulations (see Figure 2b). At a sampling time of 0.4 s the position of each ion was projected back in time by 0.4 s antiparallel to their current velocity vector. Ions whose projected locations crossed the sampling shell had their positions, velocities, and densities recorded for analysis. Any particular particle could have more than one shell crossings during the sampling time, but only one crossing (the last one) is recorded. The ion fluxes through the spherical shell were collected during the last 20 s of each simulation. The sampling shell was subdivided into the same four regions defined by *Brain et al.* [2015] and each region further subdivided into 5° × 5° bins. The ion fluxes in each bin from the first four simulations (MTCs of 0°, 90°, 180°, and 270°) are averaged together to create a "daily averaged" ion flux. The daily averaged ion flux is used to calculate the heavy ion escape rate for the simulations. The ion escape rate from the simulations is then compared to the median ion escape rate reported by *Brain et al.* [2015].

The next section addresses whether or not the simulations agree with the MAVEN observations, what the total ion escape rate for ions of all KE is, and tests the assumptions made by *Brain et al.* [2015].

4. Results

4.1. Global Ion Loss Rates (KE > 25 eV)

The objective of this paper is to determine how well Martian ion escape rates from HALFSHEL agree with the ion escape rates measured by MAVEN. A comparison of the simulation rates and the MAVEN rates are shown in Figure 4. The global ion loss rate for ions with KE > 25 eV was reported to be 2.8×10^{24} ions/s by *Brain et al.* [2015]. This loss rate was calculated using the median fluxes observed in each bin by MAVEN and is represented by the solid horizontal line in Figure 4. The dashed lines represent the range of the global loss rates using the middle 50% of the ion flux data collected by MAVEN in each bin. The first point 6.3×10^{24} ions/s is the loss rate from the daily averaged simulations with a solar wind speed of 485 km/s. The bracket bars represent two standard deviations of the scatter in the simulated loss rates (discussed later in this paper). The second point 5.7×10^{24} ions/s is the ion escape rate from the 400 km/s run adjust to represent the daily averaged ion loss. The third point 4.0×10^{24} ions/s represents the simulation results corrected for the change in the EUV flux at Mars.

The MAVEN loss rates are based on data collected over a large range of Martian MTC orientations. It is best to use daily averaged ion loss rates from the simulations to compare to the with the MAVEN results. The 400 km/s solar wind run was performed for a MTC = 270°. The heavy ion loss rate from this run was found to be 4.8×10^{24} ions/s. From the first four simulations with v_{sw} = 485 km/s, it was found that ion escape

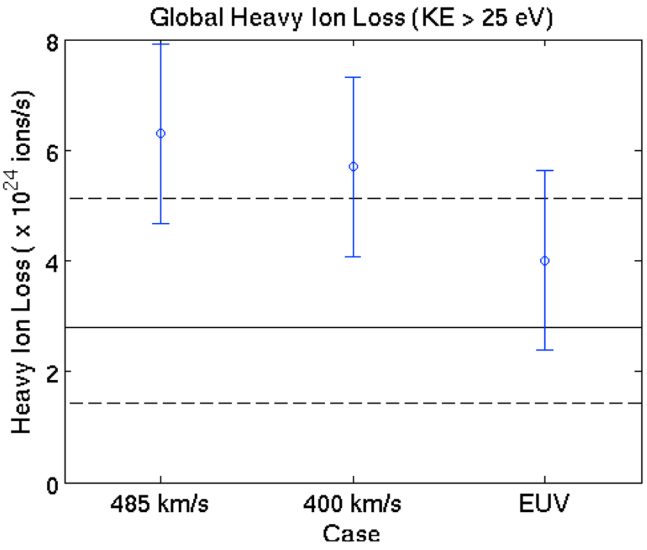

Figure 4. The global heavy ion loss rates of ions with KE > 25 eV from HALFSHEL corrected for solar wind speed and EUV flux, compared to the MAVEN results of *Brain et al.* [2015]. The solid line at 2.8×10^{24} ions/s is the net heavy ion global loss rate from MAVEN; the dashed lines represent the spread in the observations.

rate from the MTC = 270° simulation was a factor of 1.2 less than the daily averaged ion escape rate. So the 4.8×10^{24} ions/s was multiplied by 1.2 to arrive at 5.7×10^{24} ion/s shown in Figure 4.

The solar activity decreased over the course of the 4.5 month MAVEN observation time. The monthly averaged $F_{10.7}$ indices observed at Earth shows a drop from 160 at the start of the period to below 110 at the end. We make the assumption that the MAVEN results are more heavily weighted to measurements made toward the end of the data collection period and adjust the simulation results using a $F_{10.7}$ value of 120. Furthermore, while MAVEN was collecting its data Mars was moving further away from the Sun. The HALFSHEL simulations were performed with Mars located 2.07×10^{11} km from the Sun; at the end of the MAVEN collection window the Sun was located 2.18×10^{11} km from the Sun. The EUV flux at Mars falls off by $1/r^2$ as Mars moves outward from the Sun; this reduces the EUV at Mars by another 10%. The effective $F_{10.7}$ index is then 108 instead of the 130 used during the simulations. The effective $F_{10.7}$ index was then used in the ion loss rate versus EUV empirical relationship derived by *Lundin et al.* [2013]. The resulting EUV correction for the 400 km/s solar wind simulation is then 4.0×10^{24} ions/s.

The simulation error bars in Figure 4 are derived by the results shown in Figure 5. The global heavy ion loss rate from the HALFSHEL simulations for ions with KE > 25 eV crossing the samping shell at 1.35 R_M was collected every 0.4 s over a time period of 20 s. The results are shown in Figure 5. There is a spread in the data due to the rotation of Mars (a little more than factor of 2, in agreement with the results of *Ramstad et al.* [2016]). The heavy ion loss rates are at their largest when MTC = 0°, placing the largest crustal fields on the nightside of the planet. The heavy ion loss rate is smallest at MTC = 180°. Also noticeable is a variation in the loss rates collected at each 0.4 s interval for any given MTC run.

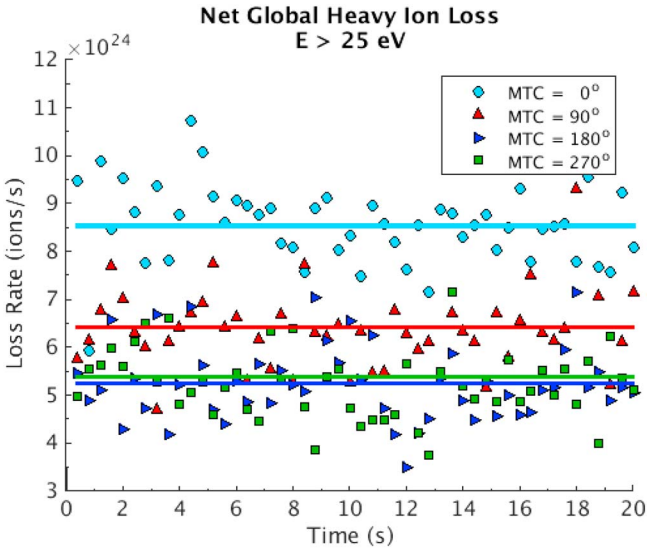

Figure 5. The figure shows the global heavy ion loss rates for ions of KE > 25 eV through a shell at 1.35 R_M collected over 20 s at the end of the run for each of the first four simulations. The horizontal lines are the mean values for each MTC angle.

The variation in the collected loss rates is due to a combination of the non-LTE chemistry and waves present in the simulations. Unfortunately, these variations cannot be detected by MAVEN during the 16 s data collection time.

They may see the effects of these reactions but cannot resolve them. The variation in the collected loss rates is much larger than would be expected due to particle statistics. Between 40 and 50 thousand particles are collected during each 0.4 s interval. The expected statistical variation is only ~0.5%, much less than the observed variation. The standard deviation for the spread in all of the loss rates shown in Figure 5 is 8.1×10^{23} ions/s. The error bars in Figure 4 are two standard deviations, representing 95.4% of the spread in the data.

The HALFSHEL loss rate of 4.0×10^{24} is within 40% of the median MAVEN result. The two data spreads overlap; the numbers are within the error bars of each other. The results are consistent with one another and could be considered in good agreement given the sources of variability in the Martian solar wind interaction previously discussed. It is possible to examine the conditions at Mars during the MAVEN observing time, derive appropriate input conditions for the simulations, and re-run them (both HAFSHEL and the MTGCM), however, that would come at a cost. The simulation results can be scaled for some of the variability detected during the 4.5 month MAVEN collected data.

For quite some time the question has been asked how do the Martian ion loss rates scale with solar wind speed, quadratically v_{sw}^2 or linearly v_{sw}? It has been postulated that the ion escape rate would scale with the solar wind dynamic pressure $\sim \rho v_{sw}^2$ [cf. *Verigin et al.*, 1997; *Kaneda et al.*, 2007; *Ma et al.*, 2014a, 2014b] or perhaps with the convection electric field $\sim v_{sw}B$. If the loss rates scale like v_{sw}^2 then the ratio between the EUV corrected loss rates would be a factor of 1.5. On the other hand, if the ion escape rates scaled with v_{sw} then the factor would be 1.2. The simulation results have a ratio of $6.3 \times 10^{24}/5.7 \times 10^{24}$ or 1.1. Two points are not enough to verify the trend. However, the result does indicate that the ion escape rate at Mars scales with the solar wind speed and hence the convection electric field. This result is consistent with the ion escape rate at Mars versus solar wind speed observations made using the MEX data by *Ramstad et al.* [2015] for solar wind densities between 0.1 and 0.5 cm^{-3}.

In summary, Figure 4 shows that the net heavy ion loss rates from the HALFSHEL simulations of the Martian solar wind interaction agree well with the MAVEN results. When the heavy ion loss rate is adjusted for the known variability in the solar wind drivers the agreement falls to within 40% of the heavy ion loss rate reported by *Brain et al.* [2015]. It was also shown that the relationship between the solar wind speed and the ion loss rate from Mars scales with v_{sw} and not v_{sw}^2 as assumed in previous studies.

4.2. Scaling the MAVEN Results via Simulations

An advantage of simulations is that they can be used to fill in the gaps in the measurements. One of the primary goals of MAVEN is to determine the total heavy ion loss rate from Mars; several assumptions and care must be made to measure and interpret the data. The limitation in the MAVEN ion loss result was the 25 eV energy cutoff used. The ion escape rates from the simulations are not limited by this energy cutoff or even where the ion fluxes are sampled. In this section the simulation results will be used to scale the MAVEN ion loss rate to account for ions of all KE.

The outward moving ion rate through the sampling shell using ions of all kinetic energies was found to be 2.0×10^{25} ions/s. The rate of the ions crossing the sampling shell moving toward the planet was found to be 2.7×10^{24} ions/s. This gives a net ion escape rate from Mars of 1.8×10^{25} ions/s. This is a factor of 4.5 larger than the 4.0×10^{24} ions/s using the 25 eV energy cutoff. One of the complexities with when using the spherical shell at 1.35 R_M is how best to deal with the inward moving ion rate. In this case the inward moving ion rate was ~14% of the outward moving ion rate. The full inward moving ion rate is subtracted from the outward moving ion rate to get the net ion escape rate from the simulations. The approach used by *Brain et al.* [2015] was more involved.

To get around dealing with the complexities of the inward moving ion rate, the ion sampling shell can be moved out. As a sanity check we construct a sampling box with six faces, of each face with an area 4 $R_M \times 4$ R_M centered on Mars. Ions crossing any of the box faces are counted and used to get the heavy ion loss rate. There are advantages to using ions at 2 R_M to calculate the ion escape rate. The ions at that distance have been accelerated for a greater distance by the electric field; they have higher kinetic energies than they do at 1.35 R_M. Thus, more ions are collected for a given energy cutoff at 2 R_M than there would be at 1.35 R_M. The second advantage is that at 2 R_M the fraction of ions moving toward Mars is significantly less than the

Table 1. Testing MAVEN Assumptions Using the Net Ion Loss Rates From the Simulations[a]

	Dayside	Nightside	$+E$	$-E$	Global
Observed outward rate ($\times 10^{24}$ ions/s)	0.23	2.02	0.22	0.27	2.74
Fraction of coverage	0.74	0.71	0.57	0.54	0.68
Scaled rate ($\times 10^{24}$ ions/s)	0.31	2.85	0.38	0.49	4.03
Full rate ($\times 10^{24}$ ions/s)	0.26	2.81	0.40	0.53	4.00
Percent diff.	+21%	+1.5%	−5.4%	−7.2%	+0.7%

[a]The first row lists the ion outflow rate from the simulation that would be observed by MAVEN. The second row is the fraction of each region sampled by MAVEN. The third row lists simulation ouflow rate that would have been sampled by MAVEN from the first row scaled up by the coverage listed in the second row to account for the unsampled regions. The fourth row contains the full ion outflow rate from each region of the simulations. The fifth row shows the percent different between the scaled ion outflow rate and the simulation ion outflow rate.

outward moving ions, a few percent or less. So there is less uncertainty in the total rate due to the returning ions. A box is used for practicality; the simulations are in Cartesian coordinates. It is more efficient to check a particle's location with respect to x, y, or z than it is to calculate the particle radius and check against that.

The rate of the ions crossing through the box was calculated and averaged using the same procedure used for the ions that crossed the sampling shell at 1.35 R_M. The difference in this case was that ions of all kinetic energies were counted, not just those with KE $>$ 25 eV. The outward moving (radially away from Mars) ion rate through the box adjusted for the change in the EUV flux was 1.7×10^{25} ions/s. The rate of the ions moving into the box (radially toward Mars) was 2.6×10^{23} ions/s or less than 2% of the outward rate.

The ratio of the global net heavy ion loss rate for the ions of all KE moving through the sampling box to the net heavy ion escape rate for ions with KE $>$ 25 eV sampled at 1.35 R_M is $1.7 \times 10^{25}/4.0 \times 10^{24} = 4.25$. Multiplying the MAVEN heavy ion escape rate by this ratio, we have 2.8×10^{24} ions/s multiplied by 3.9 producing 1.2×10^{25} ions/s.

4.3. Testing the Assumptions of *Brain et al.* [2015]

Recall the assumptions made by *Brain et al.* [2015] to derive the heavy ion escape rate for ions with KE $>$ 25 eV: (1) The sampled ion flux is on average characteristic of the unsampled regions. (2) Most of the particles traveling toward the planet on the nightside originated below the sampling shell and should be subtracted from the escape rate. (3) Ions moving radially toward the planet in the other regions originated from above the sampling shell and should not be counted as ionospheric loss.

The first assumption can be tested by using the net ion loss rates from the simulations (corrected for the solar wind speed and EUV flux) through each of the regions defined in Figure 2. The results are listed in Table 1. The outward moving ion rates for ions with KE $>$ 25 eV are calculated using the ion fluxes. Ions that cross the 1.35 R_M sampling shell are binned into the same 5° × 5° MSE latitude-longitude bins used to sort the MAVEN data. The fluxes through the bins that coincide with the bins MAVEN collected data are then used to calculate the outward moving ion rate. Those results are shown in the first row of Table 1. The fraction of each region that MAVEN collected data is listed in the second row. The third row scales the outward moving ion rate by the fraction of the area MAVEN collected data. This is done by dividing each column in the first row by each column in the second row. The fourth row shows the outward moving ion rate calculted using the total simulated ion flux for ions with KE $>$ 25 eV through each region. The fifth row shows the percent difference between the scaled rates in the fourth row and the total rates in the fifth row. Recall that the assumption was that the sampled ion fluxes (and hence ion rates) are on average characteristic of the ion fluxes through the unsampled regions. For this to be true the percent difference would be 0 if the net ion loss rates scale by area. With the exception of the dayside region this is the case to within 8%. Globally, the difference is only 0.4%.

The current simulations do not differentiate between O^+ created in the ionosphere and O^+ originating from the hot O corona. Therefore, it is difficult to use the simulations to fully test the validity of assumptions 2 and 3. However, all of the O_2^+ in the simulations is created below an altitude of 500 km, well inside the sampling shell. Thus, any inward moving O_2^+ crossing the sampling shell comes from the ionosphere and should be removed from the ion loss rate calculation. About 20% of the inward moving ion rates through the dayside and $\pm E$ regions in the simulations was O_2^+. If we assume that the same is true for

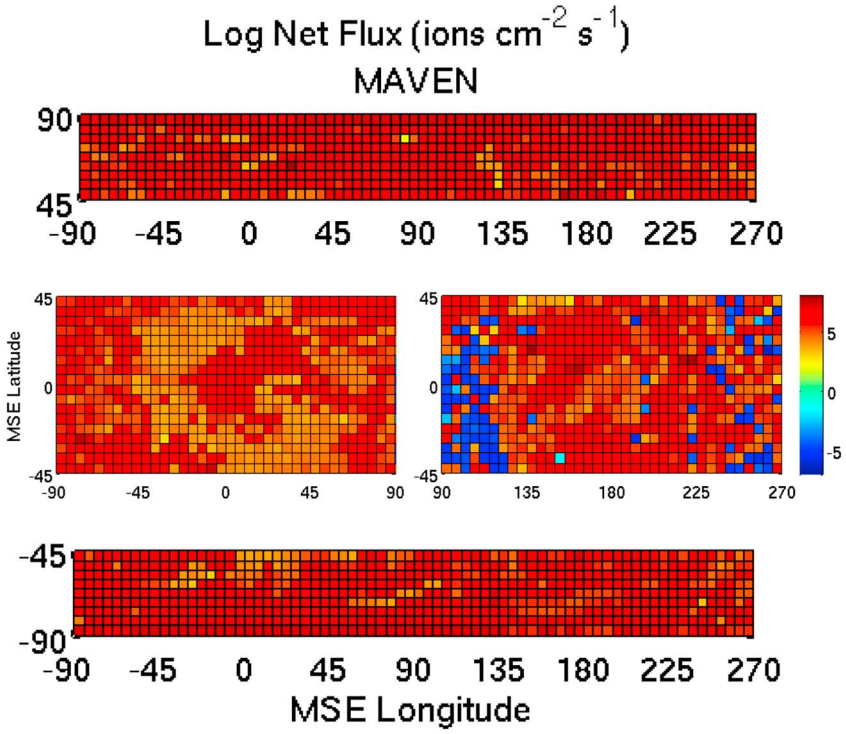

Figure 6. Net ion flux through each region defined in Figure 2 observed by MAVEN corrected for the ion flux through bins lacking MAVEN observations. Negative flux values indicate a net inward moving ion flux.

the MAVEN data then *Brain et al.* [2015] overestimated the heavy ion loss rate by 1.0×10^{23} ions/s. If roughly another 20% of the inward moving ions were due to O^+ created in the ionosphere then the reported MAVEN rate would be overestimated by 2×10^{23} ions/s. In either case the overestimation is small enough that assumption 3 does not make much of a difference.

In summary the assumption that ion flux is on average characteristic of the unsampled regions is not strictly valid on a region by region basis. However, it is valid when applied using the global average. The assumption that only the nightside inward ion flux originated from below that sampling sphere was not found to be valid, but it does not have a large impact on the heavy ion loss rate.

4.4. Net Ion Fluxes

The net ion fluxes from the MAVEN results are now compared to the daily averaged net ion fluxes. Figure 6 shows the filled in net MAVEN ion fluxes through each region defined in Figure 2. The net ion flux through each unsampled region was filled in using the following steps. The difference between the scaled up outward moving ion flux and that measured by MAVEN was 3.1×10^{24}–2.1×10^{24} or 1.0×10^{24} ion/s. We make the assumption that this ion loss rate was uniformly distributed about Mars so the loss rate was spread equally about the unsampled regions. The area of each unsampled region was then used to compute the outward ion flux through that region. The same procedure was used to fill in the inward moving ion fluxes in the nightside region. The net flux was found by taking the outward moving flux through each region and subtracting off the inward moving flux only in the nightside region.

The net flux through the dayside region is less than the net flux through the nightside region. The net flux is inward near the terminators (90° and 270°) in the nightside. A hint of a polar plume is from the $+\boldsymbol{E}$ region can be made out. The total flux through $+\boldsymbol{E}$ region is larger than the total flux through the $-\boldsymbol{E}$ region. Only a little more than 50% of the $\pm\boldsymbol{E}$ regions are sampled by MAVEN. The procedure used to fill in the missing data hides the strength of the plume. It may have been better to spread the ion loss rate based on the average loss rate sampled through each region. However, the current figure is sufficient enough to representative the net MAVEN flux data.

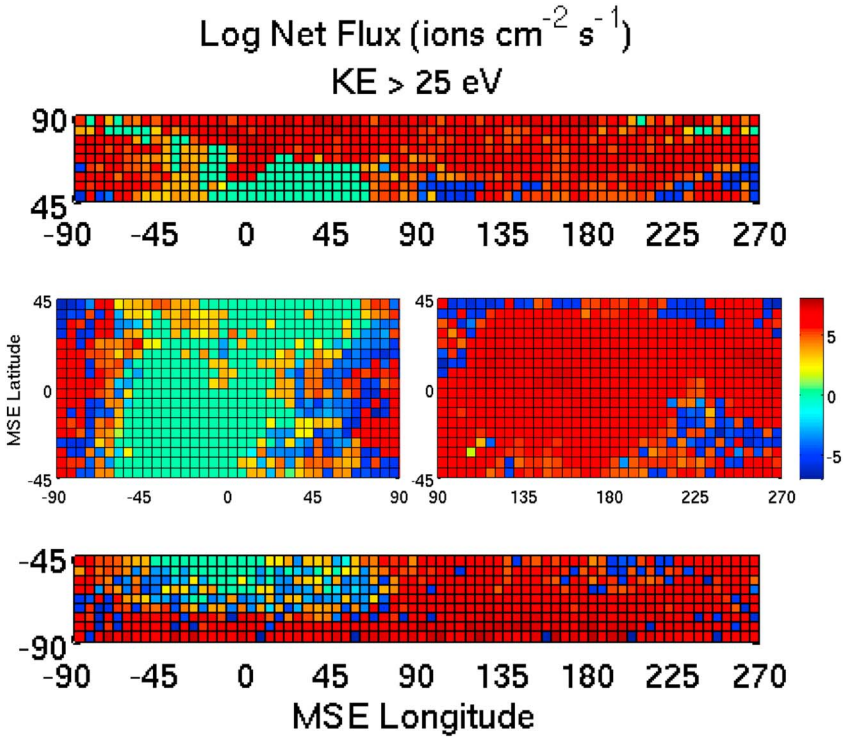

Figure 7. Net daily averaged ion flux from the simulations through each region defined in Figure 2 for ions with KE $>$ 25 eV.

The net daily averaged ion flux from the simulations is shown in Figure 7. Similar to the MAVEN results the net flux through the dayside region is less than the net flux through the nightside region. The flux through the dayside regions of the simulation is less than it is for the MAVEN data. This could be the results of the models used for the neutral atmosphere and hot O corona not having the same radial profile as the actual profiles at Mars. Future data from MAVEN's Neutral Gas and Ion Mass Spectrometer will help sort this out. The total simulated ion flux is largest in the nightside region as was the case in the MAVEN observations. The difference, however, was that the net flux was into the planet near the terminators in the MAVEN data. That is not the case for the ion flux in the nightside of the simulations. The simulations do shown a net inward flux near the terminators on the dayside of region. This difference may be the result of how the net ion flux was calculated by *Brain et al.* [2015] (only subtracting the inward flux from the nightside) or inconsistency between the neutral models used in the simulation and the actual neutral density profiles present at Mars. Figure 7 does not show any clear preference of a $+\boldsymbol{E}$ polar plume over a $-\boldsymbol{E}$ polar plume. The net ion flux from the $+\boldsymbol{E}$ region look similar to the net ion flux from the $-\boldsymbol{E}$ region. The net ion flux through the $-\boldsymbol{E}$ region was found to be altitude-dependent. Choosing a sampling shell with a radius of 1.25 R_M resulted in the net ion flux being into the planet in the $-\boldsymbol{E}$ region. Thus, the net ion flux observed by MAVEN in the $-\boldsymbol{E}$ region may be influenced by the altitude it is collected at. In contrast the net ion flux through the $+\boldsymbol{E}$ region was found to be independent of the altitude it was measured at.

It is natural to ask how the ion fluxes around Mars might change as a function of the energy cutoff used. Figure 8 shows the net ion fluxes through each region defined in Figure 2 collected through a sampling shell at 1.35 R_M using ions of all kinetic energies. The net ion flux through the nightside region is much larger, and there is no longer ion flux moving toward the planet in this region. The net ion flux through the dayside region is similar to those in Figure 7. There are some regions where the net flux pointed toward the planet that are now moving outward.

A better understanding of how the energy cutoff affects the ion flux around Mars can be examined in Figure 9. In Figure 9 the net ion flux through each sampling bin in Figure 8 was divided by the ion flux in each sampling bin of Figure 7. Dark regions are where the ion fluxes in the two figures were about equal. White bins are where the net flux shown in Figure 7 was inward. The energy cutoff does not affect the

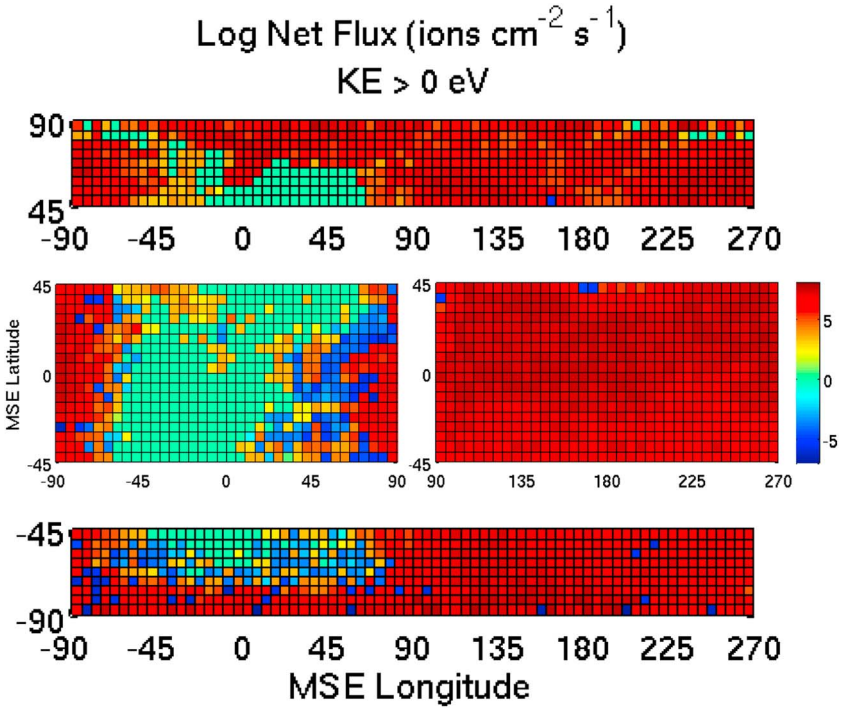

Figure 8. The daily averaged simulated net ion flux through each region defined in Figure 2 for ions with KE > 0 eV.

net ion flux through the ±***E*** region because the electric field quickly accelerates the ions originating from this region. The net ion flux through the dayside region changes near the terminators where the net flux now moves outward from the planet. The region where the energy cutoff has the largest effect is in the nightside region where the net ion flux increases 1–2 orders of magnitude. The ion fluxes are much

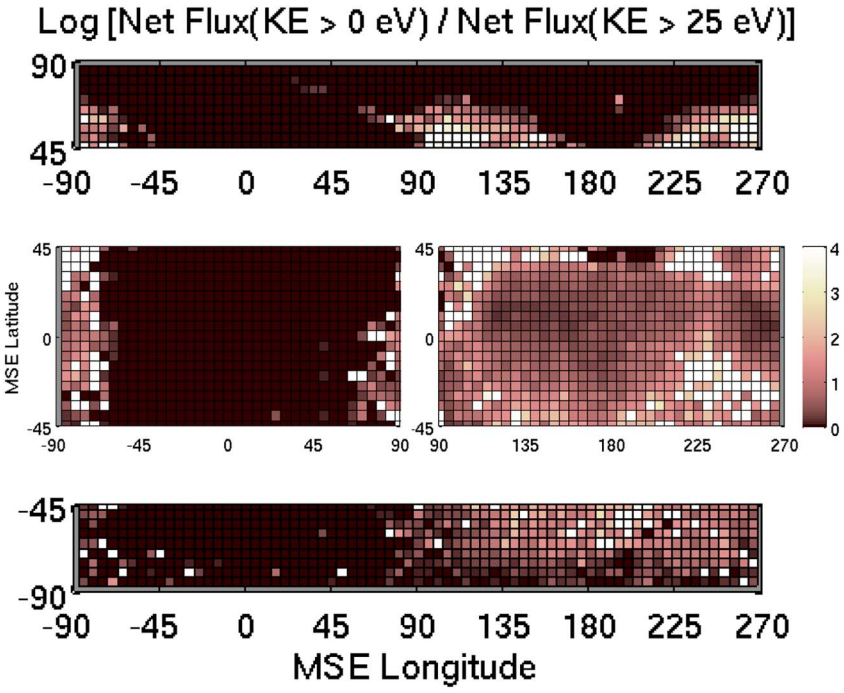

Figure 9. The ratio of the net simulated ion flux for ion with KE > 0 to the net ion flux for ions with KE > 25 through each region defined in Figure 2.

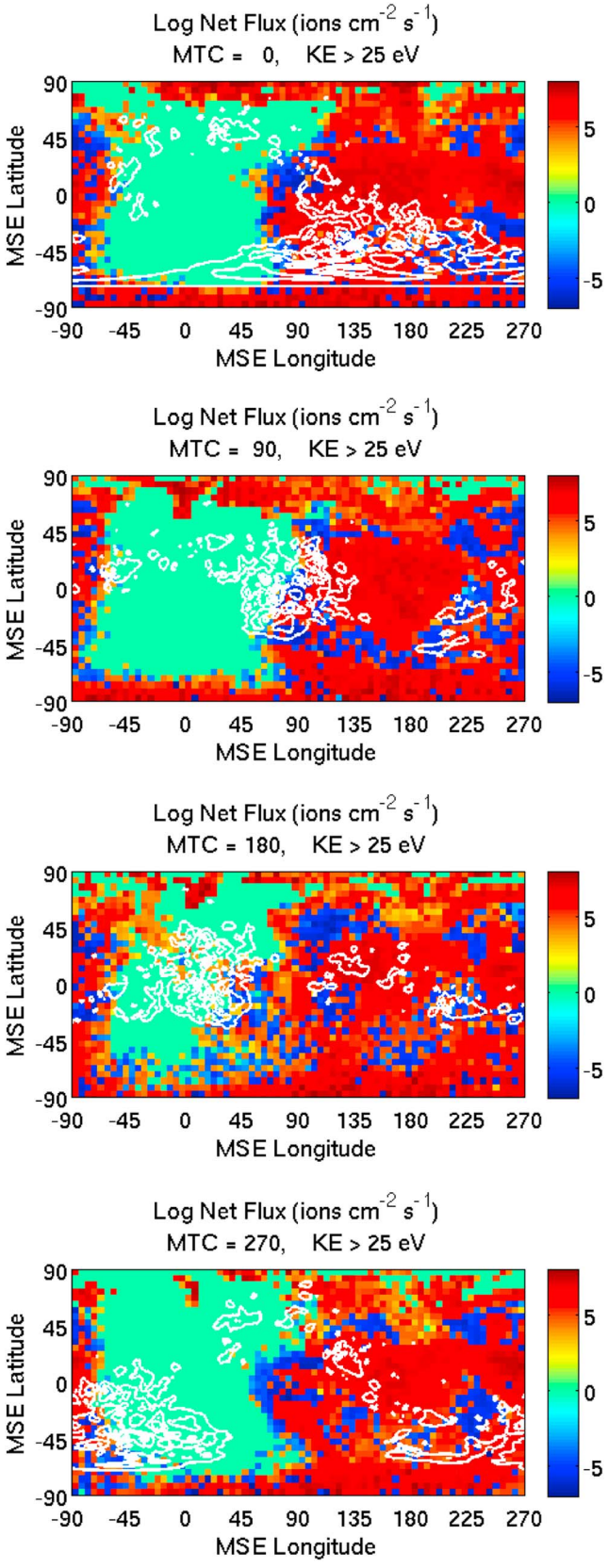

Figure 10. Net simulated ion flux versus MTC angle. Contours of the crustal magnetic field are shown in white.

larger when the energy cutoff is not applied. The low-energy ions do not have a high velocity, but they do have a larger density.

4.5. Ion Loss Versus Rotation

The results discussed here have used the daily averaged heavy ion loss rate. We take the time to mention the heavy ion loss rate for ions with KE > 0 eV versus MTC. The net heavy ion loss rates scaled for EUV and solar wind speed through the sampling box for MTCs 0°, 90°, 180°, and 270° were (1.7, 1.7, 1.5, and 1.5) × 10^{25} ions/s, respectively. This is a different ion escape rate versus MTC relationship than was found in *Brecht et al.* [2016], for L_S of 180° during solar maximum. In that case, the maximum heavy ion loss rates occurred at MTCs 90° and 180°. While *Ma et al.* [2014a, 2014b] found yet a different relationship between escape rate and rotation for solar minimum conditions. They found that most of the ions escaped when the MTC = 90°, ~2.5 × 10^{24} ions/s, followed by MTC = 270°, with 1.5 × 10^{24} ion/s escaping then 180° and 0° with 1.3 × 10^{24} ions/s and 1.2 × 10^{24} ions/s, respectively. This suggests that the role of MTC will change depending on solar activity.

The results here show a decrease in the ion loss rate when the large crustal field is at the subsolar point and at the morning terminator. In contrast MHD simulations by *Ma et al.* [2014a, 2014b] and *Fang et al.* [2015] found that the ion escape rate was enhanced when the large crustal magnetic fields were located near the dawn and dusk terminators. Observations by *Ramstad et al.* [2016] found that when the large crustal magnetic field was located between solar zenith angles of ~28°–60° the ion escape rate was its lowest. The highest ion escape rates occurred when the large crustal magnetic fields where between solar zenith angle of 60°–80°. Detailed

comparisons between the simulations and the observations are not straightforward due to uncertainties in the upstream conditions and in making the ion escape observations.

The net scaled ion flux for each MTC angle is shown in Figure 10. Contours of the crustal magnetic field are also plotted. The shape of the contours change as the planet rotates. This is because Mercator projection in the MSE system distorts the apparent shape of the crustal magnetic fields when they are near the poles.

The orientations where the large crustal fields are between ±90° at MTC = 180° and 270° is when the ion escape rate is at its minimum values. In the MTC = 180° orientation, the net outward flux increases from the dayside, but there is also more returning flux into the nightside of Mars. The outward flux from the nightside of Mars is reduced in the MTC = 270° orientation. In contrast when the large crustal fields are located in the nightside of the planet such as at MTC = 0° or the dawn terminator at MTC = 90° the return flux into the nightside of Mars is suppressed.

The results in Figure 10 illustrate the difficulty in trying to understand the how the orientation of the crustal fields effect the ion flow around Mars. The interplay between the various coordinate systems and field orientations means that things are not as simple as one may think. For instance, the large southern crustal fields may at times be found near the equator in the MSE system due to the planets' tip and rotation. Not to mention further complications that arises because of the direction of the convection electric field can have any orientation.

5. Discussion

The net heavy ion loss rates for ions with KE $>$ 25 eV from the HALFSHEL simulations of the Martian solar wind interaction agree with the rates measured by MAVEN and reported by *Brain et al.* [2015]. When the HALFSHEL rates are adjusted for changes due to the Martian orbit, solar activity and the average solar wind speed the heavy ion loss rates are within 40%.

The consistency between MAVEN and HALFSHEL implies that the MAVEN results also must agree with the empirical relationship between ion loss rate and the EUV flux, reported by *Lundin et al.* [2013]. Based on our simulation results the MAVEN results are in agreement with the ion loss rates measured by MEX and Phobos [cf, *Lundin et al.*, 2013, and references therein]. This result implies that we have a basic understanding of what are the key physical processes that drive ion escape from Mars. However, there is still work to be done to better refine our understanding of ion loss from Mars and the sensitivities to various drivers.

A better understanding of the effects the orientation of the crustal magnetic fields in the MSE coordinates system has on the ion loss rates is needed. As mentioned earlier at least half of the MAVEN observations were made when the convection electric field had a vector component pointed below the ecliptic plane. The convection electric field in the simulations was perpendicular to the ecliptic plane and pointed above it. The current simulations and others have shown that the orientation of the crustal magnetic fields (via daily rotation) affects the ion loss rates from Mars [cf. *Brecht et al.*, 2016; *Brecht and Ledvina*, 2014, 2012; *Ma et al.*, 2015, and references therein]. However, we do not know how rotating the convection electric field so that it points below the ecliptic will affect the ion loss rates. The other extreme cases when the convection electric field is parallel to the ecliptic plane also need to be examined. These are tests that will need to be done in future simulations.

The testing of the ion loss rates versus the solar wind speed indicates a linear relationship. This implies that the convection electric field is the important driver for ion loss at Mars as opposed to the solar wind dynamic pressure. *Ramstad et al.* [2016] used MEX observations to examine the relationship between solar wind speed and ion escape at Mars. They found that for low solar wind densities (0.1–0.5 cm^{-3}) and low EUV intensity the ion escape rates increased with solar wind speed. They found no increase in the ion escape rates versus solar wind speed for higher solar wind densities or EUV intensities. *Ramstad et al.* [2016] did not have information about the IMF. They could not sort their observations via the convection electric field. Further simulations and spacecraft (MAVEN and MEX) observations are needed to further test how Martian ion loss scales with the solar wind speed.

It is difficult to determine what part of the radially inward moving ion flux that MAVEN measures originates from the ionosphere versus ionization of the hot O corona. *Brain et al.* [2015] addressed this issue the simplest

way they could by just assuming that all of radially inward moving flux into the dayside was from the hot O corona. This is not strictly correct and leads to an overestimation of the heavy ion loss rate from Mars. The reported HALFSHEL simulations were not set up to determine what fraction of the inward moving ion flux through each region originates from the hot O corona versus the ionosphere. Future simulations can be set up to delineate the different O^+ sources.

The lack of an inward moving ion flux in the dayside region of the simulated ion flux maps has implications for the interpretation of the MAVEN observations. If this missing inward flux is due to a poor representation of the hot O corona ion source, then the flux MAVEN observes in this region likely originates from the hot O corona. The MAVEN flux measurements then can be used to constrain models of the corona. Future simulations together with further observations are needed to get a handle on this issue.

It would be better for MAVEN to use flux measurements from a radius larger than 1.45 R_M. Ion fluxes at larger radii have a much smaller relative inward moving ion rate compared to the outward rate. Furthermore, the electric field accelerates the ions through a larger distance. Thus, the ions tend to have a larger kinetic energy making the total ion escape rate less sensitive to the selected value of kinetic energy cutoff. The result is a much more reliable measurement of the heavy ion loss rate.

6. Summary

The HALFSHEL heavy ion loss rates for ions with KE $>$ 25 eV agree with the MAVEN results reported by *Brain et al.* [2015]. When the simulation loss rates are adjusted for changes in the orbital distance, the solar activity, and average solar wind speed the agreement is within 40% of the MAVEN rates. The ion escape rate was found to vary linearly with the solar wind speed as opposed to the solar wind dynamic pressure. Scaling the MAVEN ion escape rate to ions of all kinetic energies predicts a total heavy ion loss rate of 1.2×10^{25} ions/s. The assumptions made by *Brain et al.* [2015] to derive the ion escape rate from Mars were found to be valid. Further simulations are needed to determine what extent rotating the convection electric field will have on the ion escape rate at Mars and to determine what fraction of the inward moving ion flux originates from the ionosphere versus ionization of the hot O corona.

Acknowledgments
We would like to acknowledge the important contribution made by Stephen Bougher of the University of Michigan in providing the neutral atmosphere used in this research. S.A. Ledvina and S.H. Brecht would like to acknowledge the support from NASA contract NNH12CF43C. S.A. Ledvina would also like to acknowledge support from the MAVEN mission. The authors would like to acknowledge the computational support provided by the NASA Advanced Supercomputer facility, NAS, at NASA Ames Research Center Moffett field CA. Finally, data from which the results of this paper are taken are available upon contact with SAL or SHB.

References

Barabash, S., A. Fedorov, R. Lundin, and J. A. Sauvaud (2007), Martian atmospheric erosion rates, *Science*, *315*, 501–503.
Bößwetter, A., T. Bagdonat, U. Motschmann, and K. Sauer (2004), Plasma boundaries at Mars: A 3-D simulation study, *Ann. Geophys.*, *22*, 4363.
Benna, M., P. R. Mahaffy, J. M. Grebowsky, J. L. Fox, R. V. Ye lle, and B. M. Ja kosky (2015), First measurements of compos ition and dynamics of the Martian ionosphere by MAVEN's Neutral Gas and Ion Mass Spectrometer, *Geophys. Res. Lett.*, *42*, 8958–8965, doi:10.1002/2015GL066146.
Bougher, S. W., R. E. Dickinson, R. G. Roble, and E. C. Ridley (1988), Mars thermospheric general circulation model–Calculations for the arrival of PHOBOS at Mars, *Geophys. Res. Lett.*, *15*, 1511–514, doi:10.1029/GL015i013p01511.
Bougher, S. W., G. Keating, R. Zurek, J. Murphy, R. Haberle, J. Hollingsworth, and R. T. Clancy (1999a), Mars Global Surveyor aerobraking: Atmospheric trends and model interpretation, *Adv. Space Res.*, *23*, 1887–1897, doi:10.1016/S0273-1177(99)00272-0.
Bougher, S. W., S. Engel, R. G. Roble, and B. Foster (1999b), Comparative terrestrial planet thermospheres 2. Solar cycle variation of global structure and winds at equinox, *J. Geophys. Res.*, *104*, 16,591–16,611, doi:10.1029/1998JE001019.
Bougher, S. W., S. Engel, R. G. Roble, and B. Foster (2000), Comparative terrestrial planet thermospheres 3. Solar cycle variation of global structure and winds at solstices, *J. Geophys. Res.*, *105*, 17,669–17,692, doi:10.1029/1999JE001232.
Bougher, S. W., R. G. Roble, and T. J. Fuller-Rowell (2002), Simulations of the upper atmospheres of the terrestrial planets, in *Atmospheres in the Solar System, Comparative Aeronomy*, *Geophys. Monogr. Ser.*, vol. 130, edited by M. Mendillo, A. F. Nagy, and J. H. Waite Jr., pp. 261–288, AGU, Washington, D. C.
Bougher, S. W., S. Engel, D. P. Hinson, and J. R. Murphy (2004), MGS Radio Science electron density profiles: Interannual variability and implications for the Martian neutral atmosphere, *J. Geophys. Res.*, *109*, E03010, doi:10.1029/2003JE002154.
Bougher, S. W., J. M. Bell, J. R. Murphy, M. A. Lopez-Valverde, and P. G. Withers (2006), Polar warming in the Mars thermosphere: Seasonal variations owing to changing isolation and dust distributions, *Geophys. Res. Lett.*, *33*, L02203, doi:10.1029/2005GL024059.
Bougher, S. W., P.-L. Blelly, M. Combi, J. L. Fox, I. Mueller-Wodarg, A. Ridley, and R. G. Roble (2008), Neutral upper atmosphere and ionosphere modeling, *Space Sci. Rev.*, *139*, 107–141, doi:10.1007/s11214-008-9401-9.
Brain, D. A., et al. (2012), Comparison of global models for the escape of Martian atmospheric plasma, AGU Fall Meeting abstracts.
Brain, D. A., et al. (2015), The spatial distribution of planetary ion fluxes near Mars observed by MAVEN, *Geophys. Res. Lett.*, *42*, 9142–9148, doi:10.1002/2015GL065293.
Brecht, S. H. (1990), Magnetic asymmetries of unmagnetized planets, *Geophys. Res. Lett.*, *17*, 1243, doi:10.1029/GL017i009p01243.
Brecht, S. H., and J. R. Ferrante (1991), Global hybrid simulation of unmagnetized planets: Comparison of Venus and Mars, *J. Geophys. Res.*, *96*, 11,209–11,220, doi:10.1029/91JA00671.
Brecht, S. H., and S. A. Ledvina (2012), Control of ion loss rates from Mars during solar minimum, *Earth Planets Space*, *64*, 165–178.
Brecht, S. H., and S. A. Ledvina (2014), The role of the Martian crustal magnetic fields in controlling ionospheric loss, *Geophys. Res. Lett.*, *41*, 5340–5346, doi:10.1002/2014GL060841.

Brecht, S. H., and V. A. Thomas (1988), Multidimensional simulations using hybrid particle codes, *Comput. Phys. Commun.*, *48*, 135.
Brecht, S. H., S. A. Ledvina, and S. W. Bougher (2016), Ionospheric loss from Mars as predicted by hybrid particle simulations, *J. Geophys. Res. Space Physics*, *121*, 10,190–10,208, doi:10.1002/2016JA022548.
Brecht, S. H., S. A. Ledvina, and B. M. Jakosky (2017), The role of the electron temperature on ion loss from Mars, *J. Geophys. Res. Space Physics*, *122*, doi:10.1002/2016JA023510.
Connerney, J. E. P., J. Espley, P. Lawton, S. Murphy, J. Odom, R. Oliversen, and D. Sheppard (2014), The MAVEN magnetic field investigation, *Space Sci. Rev.*, doi:10.1007/s11214-015-0169-4.
Connerney, J. E. P., J. R. Espley, G. A. DiBraccio, J. R. Gruesbeck, R. J. Oliversen, D. L. Mitchell, J. Halekas, C. Mazelle, D. Brain, and B. M. Jakosky (2015), First results of the MAVEN magnetic field investigation, *Geophys. Res. Lett.*, *42*, 8819–8827, doi:10.1002/2015GL065366.
Cravens, T. E., A. Hoppe, S. A. Ledvina, and S. McKenna-Lawlor (2002), Pickup ions near Mars associated with escaping oxygen atoms, *J. Geophys. Res.*, *107*(A8), 1170, doi:10.1029/2001JA000125.
Curry, S. M., M. Liemohn, X. Fang, Y. Ma, J. Slavin, J. Espley, S. Bougher, and C. F. Dong (2014), Test particle comparison of heavy atomic and molecular ion distributions at Mars, *J. Geophys. Res. Space Physics*, *119*, 2328–2344, doi:10.1002/2013JA019221.
Dong, C., S. W. Bougher, Y.-J. Ma, G. Toth, A. F. Nagy, and D. Najib (2014), Solar wind interaction with Mars upper atmosphere: Results from the one-way coupling between the multifluid MHD model and the MTGCM model, *Geophys. Res. Lett.*, *41*, 2708–2715, doi:10.1002/2014GL059515.
Dong, Y., X. Fang, D. A. Brain, J. P. McFadden, J. S. Halekas, J. E. Connerney, S. M. Curry, Y. Harada, J. G. Luhmann, and B. M. Jakosky (2015), Strong plume fluxes at Mars observed by MAVEN: An important planetary ion escape channel, *Geophys. Res. Lett.*, *42*, 8942–8950, doi:10.1002/2015GL065346.
Dubinin, E., et al. (2008), Structure and dynamics of the solar wind/ionosphere interface on Mars: MEX-ASPERA-3 and MEX-MARSIS observations, *Geophys. Res. Lett.*, *35*, L11103, doi:10.1029/2008GL033730.
Fang, X., M. W. Liemohn, A. F. Nagy, J. G. Luhmann, and Y. Ma (2010a), On the effect of the Martian crustal magnetic field on atmospheric erosion, *Icarus*, *206*(1), 130–138, doi:10.1016/j.Icarus.2009.01.012.
Fang, X., M. W. Liemohn, A. F. Nagy, J. G. Luhmann, and Y. Ma (2010b), Escape probability of Martian atmospheric ions: Controlling effects of the electromagnetic fields, *J. Geophys. Res.*, *115*, A04308, doi:10.1029/2009JA014929.
Fang, X., Y. Ma, D. Brain, Y. Dong, and R. Lillis (2015), Control of Mars global atmospheric loss by the continuous rotation of the crustal magnetic field: A time-dependent MHD study, *J. Geophys. Res. Space Physics*, *120*, 10,926–10,944, doi:10.1002/2015JA021605.
Halekas, J. S., E. R. Taylor, G. Dalton, G. Johnson, D. W. Curtis, J. P. McFadden, D. L. Mitchell, R. P. Lin, and B. M. Jakosky (2013), The solar wind ion analyzer for MAVEN, *Space Sci. Rev.*, *101*, doi:10.1007/s11214-013-0029-z.
Halekas, J. S., et al. (2015), MAVEN observations of solar wind hydrogen deposition in the atmosphere of Mars, *Geophys. Res. Lett.*, *42*, 8901–8909, doi:10.1002/2015GL064693.
Harnett, E. M., and R. M. Winglee (2006), Three-dimensional multifluid simulations of ionospheric loss at Mars from nominal solar wind conditions to magnetic cloud events, *J. Geophys. Res.*, *111*, A09213, doi:10.1029/2006JA011724.
Holmstrom, M., and X.-D. Wang (2015), Mars as a comet: Solar wind interaction on a large scale, *Planet. Space Sci.*, *119*, doi:10.1016/j.pss.2015.09.017.
Jakosky, B. M., J. M. Grebowsky, J. G. Luhmann, and D. A. Brain (2015), Initial results from the MAVEN mission to Mars, *Geophys. Res. Lett.*, *42*, 8791–8802, doi:10.1002/2015GL065271.
Kallio, E., and P. Janhunen (2002), Ion escape from Mars in a quasi-neutral hybrid model, *J. Geophys. Res.*, *107*(A3), 1035, doi:10.1029/2001JA000090.
Kaneda, K., N. Terada, and S. Machida (2007), Time variation of nonthermal escape of oxygen from Mars after solar wind dynamic pressure enhancement, *Geophys. Res. Lett.*, *34*, L20201, doi:10.1029/2007GL030576.
Lammer, H., et al. (2013), Outgassing history and escape of the Martian atmosphere and water inventory, *Space Sci. Rev.*, *174*, 113–154, doi:10.1007/s11214-012-9943-8.
Lasue, J., N. Mangold, E. Hauber, S. Clifford, W. Feldman, O. Gasnault, C. Grima, S. Maurice, and O. Mousis (2013), Quantitative assessments of the Martian hydrosphere, *Space Sci. Rev.*, *174*, 155–212, doi:10.1007/s11214-012-9946-5.
Ledvina, S. A., Y.-J. Ma, and E. Kallio (2008), Modeling and simulating flowing plasmas and related phenomena, *Space Sci. Rev.*, *139*, 143–189, doi:10.1007/s11214-008-9384-6.
Liu, Y., A. F. Nagy, T. I. Gombosi, D. L. DeZeeuw, and K. G. Powell (2001), The solar wind interaction with Mars: Results of the three-dimensional three species MHD studies, *Adv. Space Res.*, *27*, 1837.
Lundin, R., S. Barabash, M. Holström, H. Nilsson, Y. Futaana, R. Ramstad, M. Yamauchi, E. Dubinin, and M. Fraenz (2013), Solar cycle effects on the ion escape from Mars, *Geophys. Res. Lett.*, *40*, 6028–6032, doi:10.1002/2013GL058154.
Ma, Y., A. F. Nagy, K. C. Hansen, and D. L. DeZeeuw (2002), Three-dimensional multispecies MHD studies of the solar wind interaction with Mars in the presence of crustal fields, *J. Geophys. Res.*, *107*(A10), 1282, doi:10.1029/2002JA009293.
Ma, Y., A. F. Nagy, I. V. Sokolov, and K. C. Hansen (2004), Three-dimensional, multispecies, high spatial resolution MHD studies of the solar wind interaction with Mars, *J. Geophys. Res.*, *109*, A07211, doi:10.1029/2003JA010367.
Ma, Y.-J., and A. F. Nagy (2007), Ion escape fluxes from Mars, *Geophys. Res. Lett.*, *34*, L08201, doi:10.1029/2006GL029208.
Ma, Y. J., X. Fang, A. F. Nagy, C. T. Russell, and G. Toth (2014a), Martian ionospheric responses to dynamic pressure enhancements in the solar wind, *J. Geophys. Res. Space Physics*, *119*, 1272–1286, doi:10.1002/2013JA019402.
Ma, Y. J., C. T. Russell, A. F. Nagy, G. Toth, J. G. Luhmann, D. A. Brain, and C. Dong (2014b), Effects of crustal field rotation on the solar wind plasma interaction with Mars, *Geophys. Res. Lett.*, *41*, 6563–6569, doi:10.1002/2014GL060785.
Ma, Y. J., et al. (2015), MHD model results of solar wind interaction with Mars and comparison with MAVEN plasma observations, *Geophys. Res. Lett.*, *42*, 9113–9120, doi:10.1002/2015GL065218.
McFadden, J. P., et al. (2015), The MAVEN Suprathermal and Thermal Ion Composition (STATIC) instrument, *Space Sci. Rev.*, *195*, 199–256.
Mitchner, M., and C. H. Kruger Jr. (1973), *Partially Ionized Gases*, chap. 4, pp. 173–182, John Wiley, New York.
Modolo, R., G. M. Chanteur, E. Dubinin, and A. P. Matthews (2005), Influence of the solar EUV flux on the Martian plasma environment, *Ann. Geophys.*, *23*, 433.
Modolo, R., et al. (2016), Mars-solar wind interaction: LatHyS, an improved parallel 3-D multispecies hybrid model, J. Geophys. Res. *Space Physics*, *121*, 6378–6399, doi:10.1002/2015JA022324.
Nilsson, H., E. Carlsson, D. A. Brain, M. Yamauchi, M. Holmstrom, S. Barabash, R. Lundin, and Y. Futaana (2010), Ion escape from Mars as a function of solar wind conditions: A statistical study, *Icarus*, *206*(1), 40–49, doi:10.1016/j.Icarus.2009.03.006.
Purucker, M., D. Ravat, H. Frey, C. Voorhies, T. Sabaka, and M. Acuna (2000), An altitude-normalized magnetic map of Mars and its interpretation, *Geophys. Res. Lett.*, *27*, 2449, doi:10.1029/2000GL000072.

Ramstad, R., S. Barabash, Y. Futaana, H. Nilsson, X. Wang, and M. Holmstrom (2015), The Martian atmophseric ion escape rate dependence on solar wind and solar EUV conditions: 1. Seven years of Mars Express observations, *J. Geophys. Res. Planets*, *120*, 1298–1309, doi:10.1003/2015JE004816.

Ramstad, R., S. Barabash, Y. Futaana, H. Nilsson, and M. Holmström (2016), Effects of the crustal magnetic fields on the Martian atmospheric ion escape rate, *Geophys. Res. Lett.*, *43*, 10,574–10,579, doi:10.1002/2016GL070135.

Verigin, M., et al. (1997), Quantitative model of the Martian magnetopause shape and its variation with the solar wind ram pressure based on Phobos 2 observations, *J. Geophys. Res.*, *102*, 2147–2155, doi:10.1029/96JA01460.